Differentially rotating strange star in general relativity

Enping Zhou,[1,2] Antonios Tsokaros,[3] Kōji Uryū,[4] Renxin Xu,[2,5] and Masaru Shibata[1,6]

[1]*Max Planck Institute for Gravitational Physics (Albert Einstein Institute), Am Mühlenberg 1, Potsdam-Golm, 14476, Germany*
[2]*State Key Laboratory of Nuclear Science and Technology and School of Physics,*
Peking University, Beijing 100871, People's Republic of China
[3]*Department of Physics, University of Illinois at Urbana-Champaign, Urbana, IL 61801, USA*
[4]*Department of Physics, University of the Ryukyus, Senbaru, Nishihara, Okinawa 903-0213, Japan*
[5]*Kavli Institute for Astronomy and Astrophysics, Peking University, Beijing, 100871, People's Republic of China*
[6]*Center for Gravitational Physics, Yukawa Institute for Theoretical Physics, Kyoto University, Kyoto, 606-8502, Japan*
(Dated: February 26, 2019)

Rapidly and differentially rotating compact stars are believed to be formed in binary neutron star merger events, according to both numerical simulations and the multi-messenger observation of GW170817. Questions that have not been answered by the observation of GW170817 and remain open are whether or not a phase transition of strong interaction could happen during a binary neutron star merger event that forms a differentially rotating strange star as a remnant, as well as the possibility of having a binary strange star merger scenario. The lifetime and evolution of such a differentially rotating star, is tightly related to the observations in the post-merger phase. Various studies on the maximum mass of differentially rotating neutron stars have been done in the past, most of which assume the so-called j-const law as the rotation profile inside the star and consider only neutron star equations of state. In this paper, we extend the studies to strange star models, as well as to a new rotation profile model. Significant differences are found between differentially rotating strange stars and neutron stars, with both the j-const law and the new rotation profile model. A moderate differential rotation rate for neutron stars is found to be too large for strange stars, resulting in a rapid drop in the maximum mass as the differential rotation degree is increased further from $\hat{A} \sim 2.0$, where $\hat{A}$ is a parameter characterizing the differential rotation rate for j-const law. As a result the maximum mass of a differentially rotating self-bound star drops *below the uniformly rotating mass shedding limit* for a reasonable degree of differential rotation. The continuous transition to the toroidal sequence is also found to happen at a much smaller differential rotation rate and angular momentum than for neutron stars. In spite of those differences, $\hat{A}$-insensitive relation between the maximum mass for a given angular momentum is still found to hold, even for the new differential rotation law. Astrophysical consequences of these differences and how to distinguish between strange star and neutron star models with future observations are also discussed.

I. INTRODUCTION

In the coming multi-messenger astronomy era led by the observation of GW170817 [1] and its electromagnetic (EM) counterparts [2], it's very likely that a conclusion could be drawn on the equation of state (EoS) of compact stars, which is a challenging topic in nuclear physics due to the non-perturbative nature of strong interaction at low energy scale. In fact, GW170817 alone has already provided ample information on the radius of neutron stars (NSs) by measuring the tidal deformability in the gravitational wave (GW) signal at the late inspiral stage (c.f. systematic studies in [3, 4]). Moreover, constraints on the maximum mass have also been put forward by considering the fate of the merger remnant together with the electromagnetic counterparts of GW170817 [5–8].

However, besides conventional NS EoSs, other possibilities such as stars composed of strange quark matter [9–11], namely strange star (SS) models, are not excluded by the observation of GW170817 [1]. In addition, the EM counterparts of GW170817 could also be understood within the scenario of a binary strange star (BSS) merger [12–15]. Because of their self-bound nature, SSs are quite different from NSs. The tidal deformability measurement from GW170817 will imply a different radius constraint if the SS branch is taken into account [16, 17]. For the case that it is supported by rigid rotation, the maximum mass of SSs can be increased much more than NSs [12]. Rotating SSs can reach much higher $T/|W|$ ratio than

NSs, leading to a more important role of triaxial instabilities for the case that the rotation is fast enough [18, 19]. Even in the case of a binary neutron star (BNS) merger, whether or not a phase transition and the formation of a SS happens during the merger will significantly alter the GW signals [20]. Considering all of the above, it's also quite important to calculate models of differentially rotating strange stars, which has never been done before, to better understand the observation of binary merger events.

Depending on the maximum mass of the EoS and the total mass of the merging binary, there could be several different outcomes after the merger: a prompt collapse to a black hole, a short-lived hypermassive neutron star (HMNS, the mass of which exceeds the mass-shedding limit with rigid rotation, hence is only stable with differential rotation) or a long-lived supramassive neutron star. The amount and the velocity of the ejected mass in the post-merger phase, the neutrino emission as well as the energy injection from the merger remnant is quite different in every case. Therefore, it's possible to make constraints on the remnant type, hence the maximum mass of the EoS, according to the EM counterparts of the merger event.

Following the evolution of a differentially rotating compact star in the post-merger phase for a long time is computationally expensive. Therefore the study of equilibrium models is very useful, especially when one is concerned with the parameter space explorations (e.g. [21, 22]). Also the evolution

of SSs is a numerically challenging problem due to its finite surface density. As a result, calculating differentially rotating SSs is an effective way to study the outcome of merger events for the hypothetical SS formation. The choice of a differential rotation law (i.e., the angular velocity as a function of the cylindrical radial coordinate $\Omega = \Omega(r \sin \theta)$ in the Newtonian case) is essential for modeling differentially rotating stars. In the case of relativistic gravity, instead, one has to choose the relativistic specific angular momentum as a function of angular velocity (i.e., $j = j(\Omega)$, in which $j := u^t u_\phi$ and u^α is the 4-velocity of the fluid). The most commonly used differential rotation law is the so-called j-const law [23–29],

$$j(\Omega) = A^2(\Omega_{\rm c} - \Omega), \tag{1}$$

in which A and $\Omega_{\rm c}$ are two constant parameters in the model. A dimensionless parameter $\hat{A} = A/r_{\rm e}$ is also quite often used, where $r_{\rm e}$ is the equatorial radius of the star. This choice results in a monotonically decreasing angular velocity with respect to the cylindrical radius. However, it has been realized that such a differential rotation profile is not realistic from numerical simulations of BNSs mergers. In the equatorial plane, simulations suggest that the angular velocity starts from a nonzero finite value on the rotational axis; then increases towards a maximum value; and then decreases to a minimum [30–35]. Hence, it's quite interesting and important to model differentially rotating stars with such a rotation law, as is done in [36].

In this paper, we have applied both the j-const law as well as a more realistic rotation law to SS models. The Compact Object CALculator (COCAL) code which we have modified to include self-bound stars and tested its convergence and accuracy before [18], is used for constructing the equilibrium solutions. We have compared our results to those of neutron stars and found that for differentially rotating SSs, both the drop of the maximum mass and the transition to the toroidal sequence happens at much larger differential rotation rate, compared with the results of NSs. Interestingly enough, the maximum mass of a differentially rotating SS can be smaller than that of a rigidly rotating one for both differential rotation laws with a reasonable differential rotation rate.

The paper is organized as follows: the SS EoSs used in this paper will be introduced in Sec.II. In Sec III we briefly review the formulations and differential rotation laws used in the calculation. The results will be presented in Sec. IV. The astrophysical implications of those results will be discussed in Sec. V. Note that in this paper we use units with $G = c = M_\odot = 1$ unless otherwise stated. Here G and c are the gravitational constant and speed of light, respectively.

II. STRANGE STAR EQUATION OF STATES

In this work, we have considered two types of EoS for SSs. One of them is the widely used MIT bag model [37]. As we are only interested in the self-bound nature of SSs and its impact of differential rotation, the effects of perturbative quantum choromodynamics (QCD) due to gluon mediated quark interactions [38–41] will not be considered, nor the finite mass of the strange quark. This allows us to have a much simpler

EoS model for numerical calculations (similar to e.g. [42]), in which pressure is related to *total energy density* according to

$$p = 1/3(\epsilon - \epsilon_s), \tag{2}$$

where $\epsilon_s = 4B$ is the total energy density at the surface and B the bag constant [10, 11]. p and ϵ are pressure and total energy density of the matter, respectively. In this work, B is chosen to be $(138 \, {\rm MeV})^4$.

Another EoS model considered in this work is the so-called strangeon star model [43]. Unlike the MIT bag model in which quarks are assumed to be de-confined and described by Fermi gas approximation, Lai and Xu suggested that clustering of quarks is possible at the density of a cold compact star since the coupling of strong interaction is not negligible at such energy scale. Lai and Xu attempted to approach the EoS with phenomenological models, i.e., to compare the potential with the interaction between inert molecules [44] (a similar approach has also been discussed in [45]). They also take the lattice effects into account as the potential could be deep enough to trap the strangeons. Combining the inter-cluster potential and the lattice thermodynamics, an EoS could be derived in terms of number density of constituent strangeon (n):

$$p = 4U_0(12.4r_0^{12}n^5 - 8.4r_0^6n^3) + \frac{1}{8}(6\pi^2)^{\frac{1}{3}}\hbar c n^{\frac{4}{3}}. \tag{3}$$

The parameters U_0 and r_0, are the depth of the potential and the characteristic range of the interaction, respectively[1]. The EoS depends also on the number of quarks in each strangeon particle ($N_{\rm q}$). Similar to the MIT bag model case, we use the rest-mass density parameter in the numerical code, which is

$$\rho = m_{\rm u} \frac{N_{\rm q}}{3} n, \tag{4}$$

where $m_{\rm u} = 931 {\rm MeV}/c^2$ is the atomic mass unit. In this work the model with $U_0 = 50 \, {\rm MeV}$ and $N_{\rm q} = 18$ is chosen. The details about the explicit implementation of SS models in the COCAL code are explained in detail in our previous work [18].

Both the MIT bag model and the strangeon star model used in this work satisfy the maximum mass constraint by the discovery of massive pulsars [18, 46, 47] as well as the tidal deformability constraint by GW170817 ([1, 13, 48], also c.f. Table.I). It's worth to remark that there is a positive correlation between the maximum mass and tidal deformabilty for NS EoSs as they both relate to the stiffness of the EoS model. According to Fig.1 in [3], in order to satisfy the tidal deformability constraint, there will be an upper limit for the maximum mass of any NS EoSs. This correlation holds qualitatively for SSs (c.f. [48, 49]) but not quantitatively due to the finite surface density of SSs which leads to a correction in the calculation of tidal deformablity [50, 51]. As a result, it's much easier for strange star models to accommodate the observation of

―――――――

[1] Note that this equation has a unique non-zero root, demonstrating the self-bound nature of strangeon star model.

EOS	ρ_{surf}	M_{TOV}	$\rho_{\mathrm{c,TOV}}$	$R_{1.4}$ [km]	$\Lambda_{1.4}$
MIT	$1.4\rho_0$	2.217	$5.42\rho_0$	11.814	792.8
LX	$2\rho_0$	3.325	$4.03\rho_0$	10.459	381.9

TABLE I. Surface density (ρ_{surf}), TOV maximum mass (M_{TOV}), central density for the TOV maximum mass solution ($\rho_{\mathrm{c,TOV}}$) for the two EOSs in this work. The densities are in units of nuclear saturation density ($\rho_0 = 2.67 \times 10^{14}\,\mathrm{g\,cm^{-3}}$). We also show the radius and tidal deformability for a 1.4 solar mass star for both EoSs.

GW170817 and massive pulsars at the same time. Additionally, previous studies have also demonstrated the possibility of understanding some puzzling observations within SS scenario, such as the energy release during pulsar glitches [52], the peculiar X-ray flares [53], the optical/UV excess of X-ray-dim isolated neutron stars [54] as well as the multiple internal plateau stages in short gamma bursts [55].

In Table.I, we list some properties of the two EoS considered in this work. The MIT bag model has a much larger ratio between central density and surface density compared with the strangeon star model for the Tolman-Oppenheimer-Volkoff (TOV) maximum mass solution (i.e., 5.42/1.4 versus 4.03/2). This result indicates that the strangeon star model is more similar to an incompressible EoS than MIT bag model quantitatively. Moreover, this difference in incompressibility will remain the same regardless of the bag constant we are using for MIT model. As pointed out by [11, 19], when neglecting strange quark mass and interaction between quarks mediated by gluons (as the model used in this paper), the properties of the maximum mass solution for both rotating and non-rotating cases simply rescale with the bag constant, keeping $\rho_{\mathrm{c}}/\rho_{\mathrm{surf}}$ unchanged. This quantitative difference between the two models will be discussed again in Sec.IV A.

III. DIFFERENTIAL ROTATION MODELS

The hydrostatic equation in equilibrium can be derived from the conservation of energy-momentum, $\nabla_\mu T^{\mu\nu} = 0$, in which $T^{\mu\nu} = (\epsilon + p)u^\mu u^\nu + pg^{\mu\nu}$ is the energy-momentum tensor of a perfect fluid. For stationary and axisymmetric differential rotating stars the Euler equation becomes [56]

$$\nabla_\mu \ln \frac{h}{u^t} + u^t u_\phi \nabla_\mu \Omega - \frac{T}{h}\nabla_\mu s = 0, \tag{5}$$

where $h = (\epsilon + p)/\rho$ is the specific enthalpy, ρ the rest mass density, T the temperature, and s the specific entropy. Assuming isentropic configurations, Eq. (5) can be integrated as

$$\frac{h}{u^t}\exp\left[\int j d\Omega\right] = \mathcal{E}, \tag{6}$$

provided an integrability condition $j := u^t u_\phi = j(\Omega)$ is assumed. $\mathcal{E}$ in Eq. (6) is a constant to be determined once the axis ratio and central density of the star is fixed.

The choice of a differential rotation law is exactly a choice for $j(\Omega)$. As explained in [56], a simple generalization of the

j-const law (Eq. (1)) is

$$j(\Omega) = A^2 \Omega\left[\left(\frac{\Omega_{\mathrm{c}}}{\Omega}\right)^q - 1\right], \tag{7}$$

where $\hat{A}$ is a parameter characterizing the differential rotation rate, Ω_{c} is the angular velocity along the rotation axis and q is a new parameter. Setting $q = 1$ one recovers the j-const law. In the COCAL code normalized coordinates are used (equatorial radius of the star is normalized to 1), thus parameter A in Eq. (7) is the same as $\hat{A}$ in other studies such as [27]. The rotation profile reduces to rigid rotation in the limit of $A \to \infty$.

Apart from the j-const law, we have also considered a more realistic differential rotation profile used in [36] which mimics the nonmonotonic Ω distribution as observed in the HMNS remnant formed in BNS simulations [34, 35]. It should be reminded that for such a nonmonotonic differential rotation profile $j(\Omega)$ becomes a multi-valued function. Hence the integrability condition is written as $\Omega = \Omega(j)$ instead. As described in [36] we use

$$\Omega = \Omega_{\mathrm{c}} \frac{1 + (j/B^2\Omega_{\mathrm{c}})^p}{1 + (j/A^2\Omega_{\mathrm{c}})^{q+p}}, \tag{8}$$

where A, B, p, and q are parameters that control the differential rotation profile. For the integration in Eq. (6), the following rearrangement is applied

$$\int j d\Omega = \int j \frac{d\Omega}{dj} dj. \tag{9}$$

The choice of (p, q) is (1,3) in our calculations. For this law, rather than fixing A and B, we choose to fix the ratio between the maximum angular velocity and the central angular velocity ($\Omega_{\mathrm{m}}/\Omega_{\mathrm{c}}$) as well as the equatorial angular velocity with respect to the central ($\Omega_{\mathrm{eq}}/\Omega_{\mathrm{c}}$) and then solve for the corresponding A and B iteratively for each solution [36].

Fixing the two angular velocity ratios mentioned above, we find that the corresponding A and B parameters vary more significantly for SSs with different central densities and axis ratios, than in NSs [36]. For solutions with large central densities or close to the mass shedding limit this affects the convergence of the method in a very delicate way. Hence, similar to what is done in [36], we concentrate on differential solutions with several constant axis ratios (i.e., $R_{\mathrm{z}}/R_{\mathrm{x}} = 0.25, 0.5$ and 0.75) instead of exploring the entire parameter space. The results will be demonstrated in the next section.

For the equations of the gravitational field we employ the Isenberg-Wilson-Mathews (IWM) formulation [57] which assumes the spatially conformal flat approximation [18]. Its validity and accuracy in calculating both rigidly rotating and differentially rotating relativistic stars has been verified in [58, 59]. According to our comparison as well as previous results, it will be useful to keep in mind that the quantities calculated and reported in this paper might have up to 2% error for global quantities (e.g. ADM mass) and up to 5% error for local quantities (e.g. angular velocity).

IV. RESULTS

In this section we present results for differentially rotating SSs both with the j-const as well as with the more realistic law Eq. (8). We focus on the properties of the maximum mass and the transition to toroidal topologies for the EoSs mentioned in Sec. II.

A. Maximum mass of differentially rotating strange star

Differentially rotating NSs could normally reach much higher maximum mass compared with uniformly rotating ones, thus called HMNS. According to previous investigations with both $\Gamma = 2$ polytropic EoS [27] or more realistic EoSs [22, 60], the maximum mass of HMNS increases as the differential rotation increases as long as the rotational profile is not extremely differential. To be precise, M_{max} increases as $\hat{A}$ decreases for various NS EoSs for $\hat{A} \in (\sim 1, \infty)$. For the case that $\hat{A}$ is smaller than 1, the maximum mass can actually drop, although it is still larger than the uniformly rotating mass shedding limit[2] (c.f. [62]). The maximum possible mass of a differentially rotating model could be as high as twice of the non-rotating maximum mass M_{TOV} [27] or even 2.5 times depending on the EoS models [63].

Regarding the maximum mass of differentially rotating star, it's important to clarify the configuration types. As first pointed out by [24], there are 4 types of differentially rotating neutron stars. For small differential rotation rate, differentially rotating star has a mass shedding limit when the star is still ellipsoidal (type A). Whereas for moderate differential rotation rates, there exists type B and C solutions, for which the maximum mass is at the toroidal limit ($R_z/R_x = 0$). The difference between type B and C is that the later can smoothly transit into an ellipsoidal sequence and eventually a spherical star by reducing angular momentum whereas the former one cannot and terminates at $R_z/R_x < 1$ when losing angular momentum. Note that when the differential rotation rate is modest, there is also type D solutions co-exists with type C solution (as type B co-exists with type A), which have two mass shedding limit but no toroidal or spherical limit. For SSs, we have found that only type C solutions exist for most of the $\hat{A}$ parameter range we considered. In another word, type A and B solutions vanishes at much smaller differential rotation rate for SSs compared with NSs. Details will be explained again in Section.IV C. There is indeed one model we have shown in Fig.1, which type A and C solutions still co-exist at different maximum density range for $\hat{A} = 5.0$ and we are showing the maximum mass of them respectively (in dash and solid). For all the other cases, without further mention, the maximum mass case is for type C configuration.

In order to investigate the maximum mass of a hypermassive strange star (HMSS) and its dependence on the $\hat{A}$ param-

eter, we have calculated HMSS models with the j-const law and various choices of $\hat{A}$ ranging from 0.6 to 6. This will enable us to make a direct comparison with the HMNS models which obey the same differential rotating law. Solutions are calculated for both the strangeon star model and MIT bag model mentioned above.

The broadbrush picture of HMSSs with j-const law is similar to that of HMNSs, but the quantitative dependence on the $\hat{A}$ parameter (namely the differential rotation rate) is quite different from what was mentioned in the paragraphs above. As $\hat{A}$ parameter approaches infinity, the rigid rotation mass shedding limit will be recovered for HMSSs. Decreasing $\hat{A}$ from infinity results to an increase of the maximum mass of HMSSs, up until $\hat{A} \sim 5$ for both strangeon star model and ~ 3 for MIT bag model (the corresponding value for HMNSs is around 1). This maximum possible mass for HMSSs is above $5\ M_\odot$. As $\hat{A}$ is further decreased from $\hat{A} \sim 5$, the maximum mass begins to decrease (as in the HMNS case). We have chosen several models with $\hat{A}$ ranging from 2 to 0.5 in Fig. 1 and Fig. 2 to better illustrate the difference compared with HMNSs with a moderate differential rotation rate.

There are several interesting points in the results shown in the figures. First of all, as pointed by [19], the maximum mass of a rigidly rotating SS (red curve) is approximately 40% larger than M_{TOV} (black curve) for both EoSs, almost twice as large as the case of NS EoSs [21]. Secondly, compared with the results of polytropic NSs with $\Gamma = 2$ shown in Fig. 1 in [27] where the maximum mass of HMNSs increases significantly from $\hat{A} = 2.0$ to 1.0, the maximum mass of HMSSs actually decreases significantly in the exactly same range of $\hat{A}$. In other words, while $\hat{A} = 2.0$ is a small differential rotation degree for NSs, it corresponds to very large one for SSs. This is understandable, considering the self-bound nature of SSs. SSs have finite surface densities which are of the same order of magnitude as the central density. In this sense, SSs are more like an incompressible star. In the case of NSs, varying the equatorial angular velocity has a smaller effect since the density at the equator approaches zero. For SSs the situation is completely different, and the configuration of the star is affected much more by differential rotation.

Another interesting feature is that HMSSs can have a smaller maximum mass than in the rigid rotation case with a moderate differential rotation rate. [3] For the strangeon star this happens at $\hat{A} \sim 1.8$ while for the MIT bag model at $\hat{A} \sim 0.7$. Two aspects can account for this very interesting result: on one hand, due to the finite surface density and larger incompressibility, the maximum mass of strange stars drops more rapidly as differential rotation is enhanced in strange stars; on the other hand, the supra-massive mass shedding limit for SSs are much larger than NSs given the same M_{TOV}, making it possible for the HMSS maximum mass to drop below it with moderate $\hat{A}$. The quantitative difference

---

[2] Neutron stars supported only by rigid rotation are called supramassive (SMNS) [61].

[3] Note that this can in principle also happen for NSs, but with unrealistically extreme differential rotation profile, e.g. $\hat{A} \sim 0.1$ for a $\Gamma = 2$ polytropic EoS.
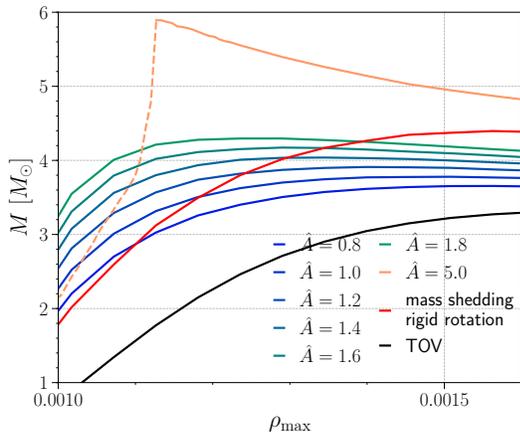
FIG. 1. Mass versus maximum density diagram for strangeon star model. The black curve is for the non-rotating case (TOV solution) while the red curve is for the mass shedding limit for uniformly rotating axisymmetric case. Curves with gradually changing color from green to blue represents the mass shedding limit for differentially rotating case with j-const law. The $\hat{A}$ parameter applied to those curves range from 1.8 to 0.8 as the color change from green to blue (from top to the bottom). Note that due to the existence of type C solutions mentioned in Sec.IV C, the maximum mass of differentially rotating case could probably be found for the case that the central density is not the maximum density inside star. We have also shown the $\hat{A} = 5$ case which corresponds to the maximum possible mass in our calculation in the yellow curve on top. For this particular differential rotation rate, type C solutions and toroidal limit are only found for large central densities (i.e., $\rho_{max} > 1.12 \times 10^{-3}$). We label the part where only type A solutions exist by dashed curve.
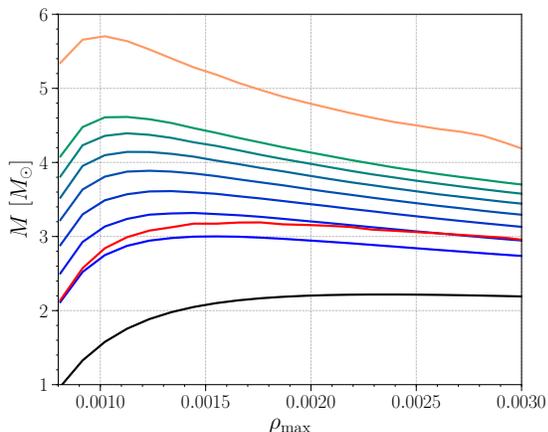

FIG. 2. Mass versus maximum density diagram for MIT bag model SSs. The models for curves with different colors are exactly the same as in Fig.1. We calculated one more model for MIT bag model with $\hat{A} = 0.6$ as shown by the bottom blue curve. The yellow curve on the top which corresponds to the maximum possible mass case for MIT bag model is with $\hat{A} = 3.0$.
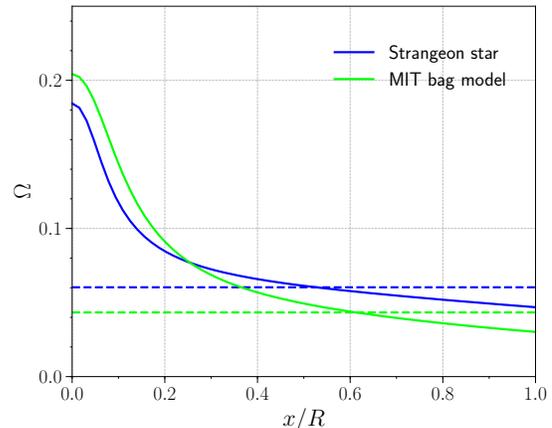

FIG. 3. The angular velocity profile for strangeon star (blue) and MIT bag model (green) when the maximum mass becomes close to their rigidly rotating mass shedding limit. This means $\hat{A} = 1.8$ for strangeon star model and $\hat{A} = 0.8$ for MIT bag model. Dashed horizontal line indicate the angular velocity for the mass shedding limit of rigid rotation case.

for MIT bag model and strangeon star model could then also be interpreted by the difference in their incompressibility, as mentioned in Sec.II. In addition, the rotational profile for the critical case where the maximum mass becomes comparable to mass shedding limit of the rigid rotation case can also be seen in Fig.3. MIT bag model indeed needs a larger physical differential rotation rate , as it has a larger Ω_c and smaller Ω_{eq}.

In order to probe the behavior above under the more realistic differential rotation law Eq. (8), we construct sequences of differentially rotating stars with deformations $R_z/R_x = 0.25$, 0.5, 0.75 in Fig. 4. The parameters are chosen such that $\Omega_m/\Omega_c = 1.1$ and $\Omega_{eq}/\Omega_c = 0.5$. Both the j-const law (dashed lines) and the new differential rotation law (solid lines) are shown for comparison. As it can be seen, with the new differential law the maximum mass is increased compared with the j-const law case. The smaller the axis ratio is (in other words, the faster the rotation), the more significant the difference between the two cases. In the case of $R_z/R_x = 0.25$, the maximum mass exceeds the mass shedding limit for rigid rotation.

However, as can be seen by comparing the 'DR-LX-I' and 'DR-LX-II' models in Table.II, the angular momentum and kinetic energy are also increased in the case of the non-monotonic differential rotation law as a trade off for a higher maximum mass. The angular momentum and kinetic energy of the merger remnant originate from the binary inspiral stage, which should be independent of the rotation law. Hence, for merger events, only comparing the remnant mass to the mass shedding limit might not be sufficient enough to tell the real outcome of the merger product, especially for the case that the remnant normally wouldn't obtain enough angular momentum to reach the mass shedding limit. In this case, investigating the relationship between the maximum mass for a given angular momentum will be particularly useful, which we will
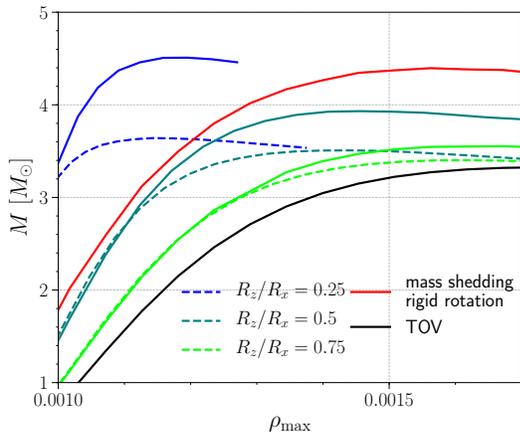
FIG. 4. Mass versus maximum density diagram for strangeon star model. The black and red curves are for non-rotating and uniformly rotating mass shedding limit case, respectively. The other curves ranging from green to blue colors are differentially rotating solutions with constant axis ratio $R_z/R_x = 0.25$, 0.5 and 0.75. The dashed curves are for models with j-const law with $\hat{A} = 1.0$ and solid curves are for models with the new rotation law Eq.(8).

explore in the next subsection.

B. Critical mass of constant angular momentum sequences

One of the most important results in the theory of stability of rigidly rotating stars is the "turning point" theorem of Friedman, Ipser, and Sorkin [64] which states that along a sequence with a constant angular momentum J and varying mass and central density, secular instability sets in at the maximum mass i.e. at the turning point of the $M - \rho$ curve. The conjecture that similar to uniformly rotating stars, the dynamical stability line also exists in differentially rotating stars was proven in the affirmative at [60] and thus the turning-point criterion can be used as a first approximation for finding the critical mass for prompt collapse to a black hole. We refer to this critical mass by M_{crit} hereafter [4].

Inspired by the fact mentioned in the previous subsection, that the maximum mass of HMSS correlates with its angular momentum, it is interesting to investigate whether HMSSs follow a similar universal relationship revealed by [22]. In particular, it has been found that the relationship between M_{crit} and J is $\hat{A}$-insensitive. Furthermore, when re-normalized by the TOV maximum mass, the relationship between dimensionless critical mass and angular momentum is found to be independent on EoSs of NSs [22]. In other words, for any NS EoSs, the enhancement in maximum mass is determined only by the angular momentum of the rotating star

but not how the angular momentum is distributed inside the star. The reason that a HMNS can have a larger maximum mass than a SMNS is because a HMNS can reach larger angular momentum. Although in [22] it has been shown that this EoS-independent relationship cannot be extended for the case of even uniformly rotating SSs, it's quite useful if one can at least verify whether the $\hat{A}$-insensitive relationship still holds for differentially rotating SSs.

We have considered the case of $\hat{A} = 1.0$ and 3.0 for both strangeon star model and MIT bag model to test the relationship between M_{crit} and J. The results are shown in Fig. 5, where the rigid rotation case (solid blue line) and the differential rotation case (colored dots) are compared. As can be seen, even though $\hat{A} = 1.0$ already represents a large differention rotation degree for SSs, the M_{crit}-J relation doesn't deviate much from the rigid rotation case (which is $\hat{A} \to \infty$) for both EoSs. The relative difference as defined in [22] satisfies

$$\frac{f_{\text{uni}} - f_{\hat{A}}}{f_{\text{uni}}} \leq 2.0\% \quad \forall \hat{A} > 1.0, \tag{10}$$

for SSs too, where f_{uni} denotes M_{crit} for a certain J for uniform rotation case and $f_{\hat{A}}$ for differential rotation case. According to the upper panel in Fig.5, the angular momentum of a differentially rotating strangeon star can reach is much smaller than that of the rigid rotating case. This explains why a HMSS could have a smaller maximum mass than SMSS. What's more interesting is that, as can be seen from the upper panel of Fig.5, the solutions with the new differential rotation law are also found to follow this relation between M_{crit} and J. This result excludes the possibility that this relationship is due to a choice of any particular differential rotation law. Hence, *one can try to infer the outcome of a binary merger event without having to know the details of the rotational profile in the merger remnant*.

C. Type C solutions of differentially rotating strange star

Another interesting and important feature of differentially rotating relativistic stars is the existence of different types of solutions according to their geometrical surface shape, namely spheroidal or toroidal classes [24]. By using COCAL, we are able to construct and study the Type C solutions of differentially rotating SSs according to the classification in [24]. For rigidly rotating relativistic stars or differentially rotating stars with relatively weak differential rotation rates, the solution sequences terminate at the so-called mass-shedding limit with a finite axis ratio R_z/R_x. Nevertheless, with a relatively strong differential rotation degree, the solution sequence could go through a continuous transition to a toroidal class with $R_z/R_x = 0$. In such solution sequences, the stellar surface in the $x - z$ plane may look like a peanut-shape and the maximum density is no longer in the center of the star but in a ring of a finite radius inside the star (c.f. Fig. 6 as an example). Identifying such solutions for differentially rotating SSs is helpful in determining the maximum mass as well as in understanding the influence of a certain differential rotation rate.

---

[4] In practice, we find M_{crit} by finding the point where $\frac{\partial M}{\partial \rho_{\text{max}}}|_J = 0$
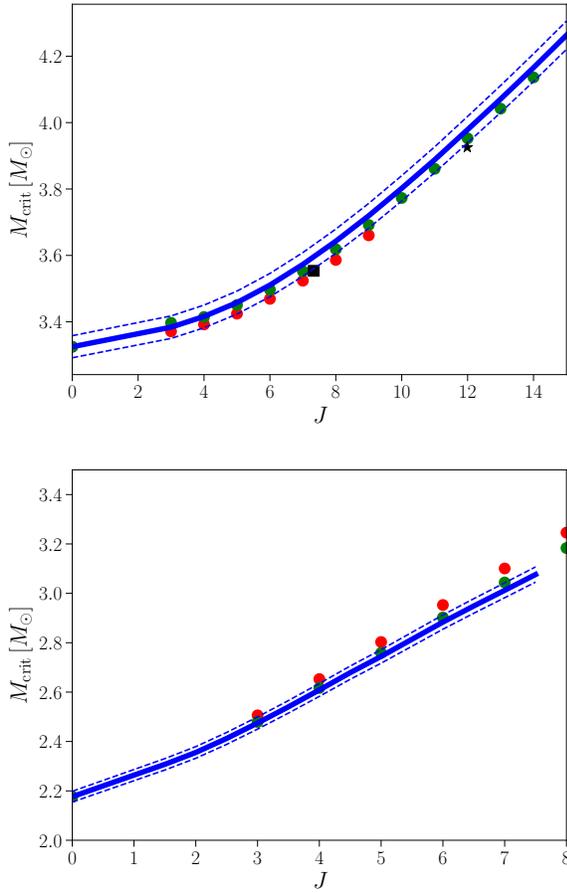
FIG. 5. The relationship between critical mass $M_{\rm crit}$ and angular momentum J for strangeon stars (upper panel) and MIT bag model stars (lower panel). Both rigid rotating case (solid blue line) and differentially rotating case (green dots for $\hat{A} = 3.0$ and red dots for $\hat{A} = 1.0$) are shown. The 1% error range for the relationship of the rigid rotating case is shown in dashed blue lines for comparison purpose. As can be seen, for both EoSs even in the case of $\hat{A} = 1.0$, the relationship between $M_{\rm crit}$ and J is still reasonable consistent with the rigid rotating case. In the upper panel, we have also labeled the results from the new differential rotation law with black markers.

According to the parameter study for the solution space of differentially rotating NSs [25], type C solutions come to exist for $\hat{A} \lesssim 1.0$ [5], although a more precise value depends on the central density. In order to make a comparison we have also tested the j-const law for SSs. Properties of selected type C solutions for differentially rotating SSs are listed in Tab. II. It turns out that type C solutions emerge at much larger $\hat{A}$, thus much smaller differential rotation rate. For instance, for both strangeon star and MIT bag model with $\hat{A} = 3.0$ (which corresponds to $\tilde{A} = 1/3$ in Fig. 5 in [25]), toroidal
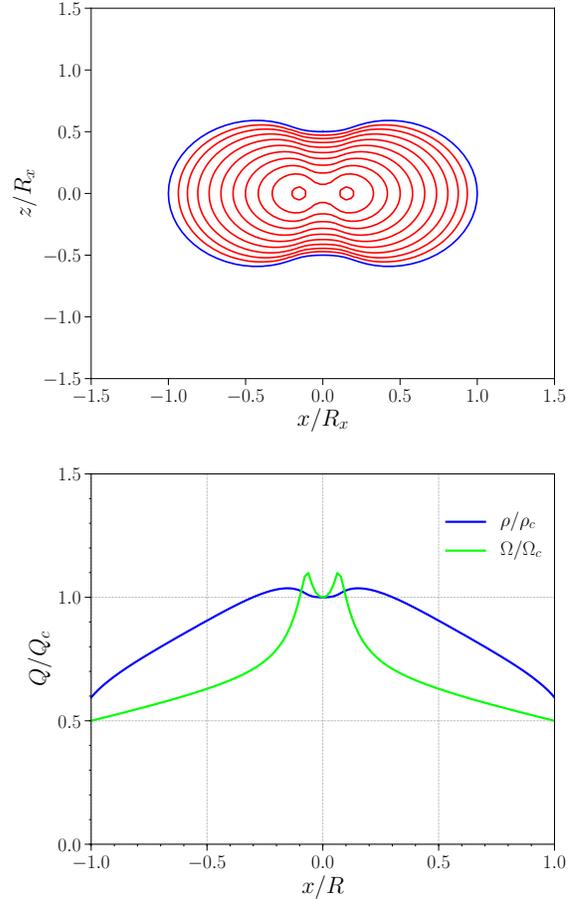
FIG. 6. Stellar surface and rest mass density contour of a differentially rotating strangeon star (upper panel) and its density and angular velocity profile (lower panel). Details about the solution shown in this figure can be found in the 'DR-LX-4' model in Table.II

solutions are already found for the whole central density range we considered.

We have identified the first solution in a sequence, the maximum density of which is no longer at the center of the star, as the beginning of the transition to the toroidal class [6]. By doing so, we realize that the transition happens at an axis ratio very close to 1 for differentially rotating SSs with $\hat{A} = 1$. In other words, with very little angular momentum, the differential rotation is already playing an important role in the changing of the configuration of a SS. One such solution is also listed as 'DR-LX-3' in Tab. II to illustrate the onset of this transition.

Similar analysis has been conducted for the solutions with the new differential rotation law. Although as mentioned above, it's not easy to have a solution with very small axis ratio as it's increasingly difficult to adopt the A and B parameter for smaller axis ratios. Despite of that, we still managed

---

[5] Note that in [25] the definition of $\tilde{A}$ is different from $\hat{A}$ used in this paper, but are related simply as $\tilde{A} = 1/\hat{A}$.

[6] Identically, one can also try to find the first solution, the surface of which in the $x - z$ plane is no longer elliptical.

to reach $R_z/R_x = 0$ and find toroidal solutions for the low central density sequence for the case used in our calculation ($\Omega_m/\Omega_c = 1.1$ and $\Omega_{eq}/\Omega_c = 0.5$). For relatively large central density sequence, we attempt to figure out whether the transition to toroidal class is already triggered by looking at the stellar surface and density profile of the star. The result shows that for $R_z/R_x = 0.5$ case, the onset of the transition already happens for all the central density range (an example can be found in Fig.6). Hence, this type C solution should be a common feature for differentially rotating relativistic stars, regardless of the EoSs and details of the rotation profile.

V. DISCUSSION AND CONCLUSION

In this paper, we have calculated differentially rotating SSs, with both MIT bag model and strangeon star model. Besides the widely used j-const law, we have also considered a more realistic non-monotonic rotation profile. The maximum mass of HMSSs, toroidal solutions and the relationship between the critical mass and angular momentum are investigated and compared with previous results of HMNSs. Two major differences are found between HMNSs and HMSSs: first, with a moderate differential rotation rate, the maximum mass of a HMNS is increased significantly as the $\hat{A}$ parameter decreases (from 2.0 to 1.0). Whereas in the same range, the maximum mass of a HMSS drops significantly. In particular, the maximum mass drops below the rigid rotation case with a moderate differential rotation rate. Secondly, the continuous transition to the toroidal solutions happens at much larger $\hat{A}$, i.e. much smaller differential rotation rate (typically $\hat{A} = 3.0$ compared with $\hat{A} = 1.0$ in the case of NSs). Both differences indicate that a moderate differential rotation degree for NSs is already too large for SSs. The self-bound nature of SSs can account for this difference, as a certain difference in the angular velocity will play a more important role for SSs, the density of which is almost uniform inside the star. Despite these differences, similarly to NSs, a universal relationship between M_{crit} and J is found for SSs, even for the new differential rotation law. This provides a more realistic way to interpret the outcome of a binary merger event, rather than compare the remnant mass with the maximum mass.

Combining all the results we have obtained in this paper, one conclusion we can draw on the differentially rotating SS

remnant formed in a binary merger event is that it's most likely to be a type C solution whose maximum density is not at the center. Meanwhile, due to the self-bound nature, the moment of inertia of SSs is larger than NSs and hence the $T/|W|$ ratio (similar results have already been reported in [18] and the resulting secular instability for uniformly rotating SSs are studied). According to previous studies on the dynamical instabilities [65–68] of differentially rotating NSs, for the extremely differential rotation rate cases (especially for the case the maximum density is no longer in the center, c.f. the discussions in [66]), the $T/|W|$ ratio for onset of such dynamical instabilities could be reduced significantly. Consequently, such instabilities may easily take place if a differentially rotating SS is formed in a binary merger, redistributing matter and angular momentum inside the star and destroying the toroidal shape of the star in a few central rotation periods, thus producing additional signatures in the GW radiation of the post-merger phase. At the same time, such instability will compete against other mechanism such as magnetorotational instability in dissipating the differential rotation, whereas the later one is known to be responsible to enhance magnetic field of the merger remnant with the differential rotational kinetic energy. Therefore, the remnant SS might have significantly smaller dipole magnetic fields compared with a NS remnant scenario, providing a way to distinguish between a BSS and BNS merger scenario with the EM counterparts.

[1] B. P. Abbott *et al.* (LIGO Scientific Collaboration and Virgo Collaboration), Phys. Rev. Lett. **119**, 161101 (2017).

[2] The LIGO Scientific Collaboration, the Virgo Collaboration, B. P. Abbott, R. Abbott, T. D. Abbott, F. Acernese, K. Ackley, C. aAdams, T. Adams, P. Addesso, and et al. (LIGO Scientific Collaboration and Virgo Collaboration), Astrophys. J. Lett. **848**, L12 (2017).

[3] E. Annala, T. Gorda, A. Kurkela, and A. Vuorinen, Physical Review Letters **120**, 172703 (2018), arXiv:1711.02644 [astro-ph.HE].

[4] B. P. Abbott, R. Abbott, T. D. Abbott, F. Acernese, K. Ackley, C. Adams, T. Adams, P. Addesso, R. X. Adhikari, V. B. Adya, and et al., Physical Review Letters **121**, 161101 (2018), arXiv:1805.11581 [gr-qc].

[5] L. Rezzolla, E. R. Most, and L. R. Weih, Astrophys. J. Lett. **852**, L25 (2018), arXiv:1711.00314 [astro-ph.HE].

[6] M. Ruiz, S. L. Shapiro, and A. Tsokaros, Phys. Rev. D **97**, 021501 (2018), arXiv:1711.00473 [astro-ph.HE].

[7] M. Shibata, S. Fujibayashi, K. Hotokezaka, K. Kiuchi, K. Kyutoku, Y. Sekiguchi, and M. Tanaka, Phys. Rev. D **96**, 123012

Model	R_x	R_z/R_x	ρ_c	$\rho_{\max}$	Ω_c	M_{ADM}	J	$T/|W|$
UR-LX	4.82 (15.1)	0.53125 (0.584)	1.56×10^{-3}	1.56×10^{-3}	0.0603	4.39	16.4	0.222
DR-LX-1	4.36 (12.4)	0.015625 (0.0190)	8.68×10^{-4}	1.51×10^{-3}	0.382	3.78	10.3	0.183
DR-LX-2	4.07 (14.4)	0.25 (0.295)	1.20×10^{-3}	1.40×10^{-3}	0.110	4.49	17.6	0.290
DR-LX-3	4.83 (10.9)	0.9375 (0.947)	1.51×10^{-3}	1.51×10^{-3}	0.0638	3.25	2.28	0.0135
DR-LX-4	4.26 (12.8)	0.50 (0.553)	1.46×10^{-3}	1.51×10^{-3}	0.0945	3.92	11.9	0.203
UR-MIT	8.23 (15.1)	0.484375 (0.523)	1.76×10^{-3}	1.76×10^{-3}	0.0433	3.17	8.56	0.198
DR-MIT-1	6.79 (13.9)	0.015625 (0.0172)	6.07×10^{-3}	1.34×10^{-3}	0.163	3.60	10.8	0.236

TABLE II. Quantities of selected solutions for rotating SSs. In the above, R_x is the coordinate (proper) equatorial radius and R_z/R_x is the ratio of coordinate (proper) polar to the equatorial radius. ρ_c is the central rest-mass density and $\rho_{\max}$ the maximum rest-mass density in the star. Ω_c, M_{ADM}, J, and $T/|W|$ are the central angular velocity, Arnowit-Deset-Misner mass, angular momentum and ratio between kinetic energy and gravitational potential. Definitions can be found in the Appendix of [56]. In this table, 'UR-LX' and 'UR-MIT' labels the maximum mass solution of uniformly rotating strangeon star and MIT bag model star, respectively. 'DR-LX-1' and 'DR-MIT-1' are the maximum mass solutions for differentially rotating strangeon star and MIT bag model star with $\hat{A} = 1$ $j-$const law. 'DR-LX-2' is the maximum mass solution for the new differential rotation law with $R_z/R_x = 0.25$ for the strangeon star model. 'DR-LX-3' and 'DR-LX-4' are two selected type-C solutions with $j-$ const law and the new differential rotation law, respectively.

(2017), arXiv:1710.07579 [astro-ph.HE].

[8] A. Bauswein, O. Just, H.-T. Janka, and N. Stergioulas, Astrophys. J. Lett. **850**, L34 (2017), arXiv:1710.06843 [astro-ph.HE].

[9] E. Farhi and R. L. Jaffe, Phys. Rev. D **30**, 2379 (1984).

[10] C. Alcock, E. Farhi, and A. Olinto, Astrophys. J. **310**, 261 (1986).

[11] P. Haensel, J. L. Zdunik, and R. Schaefer, Astron. Astrophys. **160**, 121 (1986).

[12] A. Li, B. Zhang, N.-B. Zhang, H. Gao, B. Qi, and T. Liu, Phys. Rev. D **94**, 083010 (2016), arXiv:1606.02934 [astro-ph.HE].

[13] X.-Y. Lai, Y.-W. Yu, E.-P. Zhou, Y.-Y. Li, and R.-X. Xu, Research in Astronomy and Astrophysics **18**, 024 (2018), arXiv:1710.04964 [astro-ph.HE].

[14] A. Bauswein, H.-T. Janka, R. Oechslin, G. Pagliara, I. Sagert, J. Schaffner-Bielich, M. M. Hohle, and R. Neuhäuser, Phys. Rev. Lett. **103**, 011101 (2009), arXiv:0812.4248.

[15] L. Paulucci, J. E. Horvath, and O. Benvenuto, in *International Journal of Modern Physics Conference Series*, International Journal of Modern Physics Conference Series, Vol. 45 (2017) p. 1760042.

[16] G. Montana, L. Tolos, M. Hanauske, and L. Rezzolla, arXiv e-prints (2018), arXiv:1811.10929 [astro-ph.HE].

[17] E. R. Most, L. R. Weih, L. Rezzolla, and J. Schaffner-Bielich, Physical Review Letters **120**, 261103 (2018), arXiv:1803.00549 [gr-qc].

[18] E. Zhou, A. Tsokaros, L. Rezzolla, R. Xu, and K. Uryū, Phys. Rev. D **97**, 023013 (2018), arXiv:1711.00198 [astro-ph.HE].

[19] D. Gondek-Rosińska, T. Bulik, L. Zdunik, E. Gourgoulhon, S. Ray, J. Dey, and M. Dey, Astron. Astrophys. **363**, 1005 (2000), astro-ph/0007004.

[20] E. R. Most, L. J. Papenfort, V. Dexheimer, M. Hanauske, S. Schramm, H. Stöcker, and L. Rezzolla, arXiv e-prints (2018), arXiv:1807.03684 [astro-ph.HE].

[21] C. Breu and L. Rezzolla, Mon. Not. R. Astron. Soc. **459**, 646 (2016), arXiv:1601.06083 [gr-qc].

[22] G. Bozzola, N. Stergioulas, and A. Bauswein, Mon. Not. R. Astron. Soc. **474**, 3557 (2018), arXiv:1709.02787 [gr-qc].

[23] H. Komatsu, Y. Eriguchi, and I. Hachisu, Mon. Not. R. Astron. Soc. **237**, 355 (1989).

[24] M. Ansorg, D. Gondek-Rosińska, and L. Villain, Mon. Not. R. Astron. Soc. **396**, 2359 (2009), arXiv:0812.3347 [gr-qc].

[25] D. Gondek-Rosińska, I. Kowalska, L. Villain, M. Ansorg, and M. Kucaba, Astrophys. J. **837**, 58 (2017), arXiv:1609.02336 [astro-ph.HE].

[26] A. M. Studzińska, M. Kucaba, D. Gondek-Rosińska, L. Villain, and M. Ansorg, Mon. Not. R. Astron. Soc. **463**, 2667 (2016).

[27] T. W. Baumgarte, S. L. Shapiro, and M. Shibata, Astrophys. J. **528**, L29 (2000).

[28] I. A. Morrison, T. W. Baumgarte, and S. L. Shapiro, Astrophys. J. **610**, 941 (2004), astro-ph/0401581.

[29] J. D. Kaplan, C. D. Ott, E. P. O'Connor, K. Kiuchi, L. Roberts, and M. Duez, Astrophys. J. **790**, 19 (2014), arXiv:1306.4034 [astro-ph.HE].

[30] M. Shibata, K. Taniguchi, and K. Uryū, Phys. Rev. D **71**, 084021 (2005), gr-qc/0503119.

[31] K. Hotokezaka, K. Kiuchi, K. Kyutoku, T. Muranushi, Y.-i. Sekiguchi, M. Shibata, and K. Taniguchi, Phys. Rev. D **88**, 044026 (2013), arXiv:1307.5888 [astro-ph.HE].

[32] T. Dietrich, S. Bernuzzi, M. Ujevic, and B. Brügmann, Phys. Rev. D **91**, 124041 (2015), arXiv:1504.01266 [gr-qc].

[33] A. Bauswein and N. Stergioulas, Phys. Rev. D **91**, 124056 (2015), arXiv:1502.03176 [astro-ph.SR].

[34] W. Kastaun and F. Galeazzi, Phys. Rev. D **91**, 064027 (2015), arXiv:1411.7975 [gr-qc].

[35] M. Hanauske, K. Takami, L. Bovard, L. Rezzolla, J. A. Font, F. Galeazzi, and H. Stöcker, Phys. Rev. D **96**, 043004 (2017), arXiv:1611.07152 [gr-qc].

[36] K. Uryū, A. Tsokaros, L. Baiotti, F. Galeazzi, K. Taniguchi, and S. Yoshida, Phys. Rev. D **96**, 103011 (2017), arXiv:1709.02643 [astro-ph.HE].

[37] A. Chodos, R. L. Jaffe, K. Johnson, C. B. Thorn, and V. F. Weisskopf, Phys. Rev. D **9**, 3471 (1974).

[38] E. S. Fraga, R. D. Pisarski, and J. Schaffner-Bielich, Phys. Rev. D **63**, 121702 (2001), hep-ph/0101143.

[39] M. Alford, M. Braby, M. Paris, and S. Reddy, Astrophys. J. **629**, 969 (2005), nucl-th/0411016.

[40] A. Li, Z.-Y. Zhu, and X. Zhou, Astrophys. J. **844**, 41 (2017).

[41] S. Bhattacharyya, I. Bombaci, D. Logoteta, and A. V. Thampan, Mon. Not. R. Astron. Soc. **457**, 3101 (2016), arXiv:1601.06120 [astro-ph.HE].

[42] F. Limousin, D. Gondek-Rosińska, and E. Gourgoulhon, Phys. Rev. D **71**, 064012 (2005), gr-qc/0411127.

[43] X. Y. Lai and R. X. Xu, in *Journal of Physics Conference Series*, Journal of Physics Conference Series, Vol. 861 (2017) p.

012027, arXiv:1701.08463 [astro-ph.HE].

[44] X. Y. Lai and R. X. Xu, Mon. Not. R. Astron. Soc. **398**, L31 (2009), arXiv:0905.2839 [astro-ph.HE].

[45] Y.-J. Guo, X.-Y. Lai, and R.-X. Xu, Chinese Physics C **38**, 055101 (2014).

[46] P. B. Demorest, T. Pennucci, S. M. Ransom, M. S. E. Roberts, and J. W. T. Hessels, Nature **467**, 1081 (2010), arXiv:1010.5788 [astro-ph.HE].

[47] J. Antoniadis, P. C. C. Freire, N. Wex, T. M. Tauris, R. S. Lynch, and et al., Science **340**, 448 (2013), arXiv:1304.6875 [astro-ph.HE].

[48] E.-P. Zhou, X. Zhou, and A. Li, Phys. Rev. D **97**, 083015 (2018), arXiv:1711.04312 [astro-ph.HE].

[49] X. Lai, E. Zhou, and R. Xu, arXiv e-prints (2018), arXiv:1811.00193 [astro-ph.HE].

[50] T. Damour and A. Nagar, Phys. Rev. D **80**, 084035 (2009), arXiv:0906.0096 [gr-qc].

[51] S. Postnikov, M. Prakash, and J. M. Lattimer, Phys. Rev. D **82**, 024016 (2010), arXiv:1004.5098 [astro-ph.SR].

[52] E. P. Zhou, J. G. Lu, H. Tong, and R. X. Xu, Mon. Not. R. Astron. Soc. **443**, 2705 (2014), arXiv:1404.2793 [astro-ph.HE].

[53] R. Xu and E. Liang, Science in China: Physics, Mechanics and Astronomy **52**, 315 (2009), arXiv:0811.0234.

[54] W. Wang, J. Lu, H. Tong, M. Ge, Z. Li, Y. Men, and R. Xu, Astrophys. J. **837**, 81 (2017), arXiv:1603.08288 [astro-ph.HE].

[55] S.-J. Hou, T. Liu, R.-X. Xu, H.-J. Mu, C.-Y. Song, D.-B. Lin, and W.-M. Gu, Astrophys. J. **854**, 104 (2018), arXiv:1710.04355 [astro-ph.HE].

[56] K. Uryū, A. Tsokaros, F. Galeazzi, H. Hotta, M. Sugimura, K. Taniguchi, and S. Yoshida, Phys. Rev. D **D93**, 044056 (2016).

[57] J. Isenberg and J. Nester, in *General Relativity and Gravitation. Vol. 1. One hundred years after the birth of Albert Einstein. Edited by A. Held. New York, NY: Plenum Press, p. 23, 1980*, Vol. 1, edited by A. Held (1980) p. 23.

[58] G. B. Cook, S. L. Shapiro, and S. A. Teukolsky, Phys. Rev. D **53**, 5533 (1996), gr-qc/9512009.

[59] P. Iosif and N. Stergioulas, General Relativity and Gravitation **46**, 1800 (2014), arXiv:1406.7375 [gr-qc].

[60] L. R. Weih, E. R. Most, and L. Rezzolla, Mon. Not. R. Astron. Soc. **473**, L126 (2018), arXiv:1709.06058 [gr-qc].

[61] G. B. Cook, S. L. Shapiro, and S. A. Teukolsky, Astrophys. J. **398**, 203 (1992).

[62] L. Rezzolla and O. Zanotti, *Relativistic Hydrodynamics* (Oxford University Press, Oxford, UK, 2013).

[63] P. Espino and V. Paschalidis, (2019), arXiv:1901.05479 [astro-ph.HE].

[64] J. L. Friedman, J. R. Ipser, and R. D. Sorkin, Astrophys. J. **325**, 722 (1988).

[65] J. M. Centrella, K. C. B. New, L. L. Lowe, and J. D. Brown, Astrophys. J. **550**, L193 (2001), astro-ph/0010574.

[66] M. Saijo, T. W. Baumgarte, and S. L. Shapiro, Astrophys. J. **595**, 352 (2003), astro-ph/0302436.

[67] M. Shibata, S. Karino, and Y. Eriguchi, Mon. Not. R. Astron. Soc. **334**, L27 (2002), gr-qc/0206002.

[68] M. Shibata, S. Karino, and Y. Eriguchi, Mon. Not. R. Astron. Soc. **343**, 619 (2003), astro-ph/0304298.